SANDIA REPORT
SAND2012-3006
Unlimited Release
April 2012

Localized Temperature Stability in Low Temperature Cofired Ceramics (LTCC)

Steve X. Dai and Lung-Hwa Hsieh

Prepared by
Sandia National Laboratories
Albuquerque, New Mexico 87185 and Livermore, California 94550

Sandia National Laboratories is a multi-program laboratory managed and operated by Sandia Corporation, a wholly owned subsidiary of Lockheed Martin Corporation, for the U.S. Department of Energy's National Nuclear Security Administration under contract DE-AC04-94AL85000.

Issued by Sandia National Laboratories, operated for the United States Department of Energy by Sandia Corporation.

Available to DOE and DOE contractors from
U.S. Department of Energy
Office of Scientific and Technical Information
P.O. Box 62
Oak Ridge, TN 37831

Telephone: (865) 576-8401
Facsimile: (865) 576-5728
E-Mail: reports@adonis.osti.gov
Online ordering: http://www.osti.gov/bridge

Available to the public from
U.S. Department of Commerce
National Technical Information Service
5285 Port Royal Rd.
Springfield, VA 22161

Telephone: (800) 553-6847
Facsimile: (703) 605-6900
E-Mail: orders@ntis.fedworld.gov
Online order: http://www.ntis.gov/help/ordermethods.asp?loc=7-4-0#online

SAND2012-3006
Unlimited Release
April 2012

Localized Temperature Stability in Low Temperature Cofired Ceramics (LTCC)

Steve X. Dai* and Lung-Hwa Hsieh[#]
*01832, Advanced Prototyping S&T
[#]5353, Radar Fuzing Department
Sandia National Laboratories
P.O. Box 5800
Albuquerque, New Mexico 87185-MS0959

Abstract

The base d ielectrics of commercial low tem perature cofired ceram ics (LTCC) systems have a temperature coefficient of resonant frequency (τ_f) in the range -50 ~ -80 ppm/°C. In this research we explored a method to realize zero or near zero τ_f resonators by incorporating τ_f compensating materials locally into a multilayer LTCC structure. To select composition for τ_f adjustment, τ_f compensating m aterials with different amount of t itanates were form ulated, synthesized, and characterized. Chemical interactions and physic al compatibility between the τ_f modifiers and the host LTCC diele ctrics were i nvestigated. Studies on stripline (SL) resonator panels with multiple compensating dielectrics revealed that: 1) co mpositions using $SrTiO_3$ provide the largest τ_f adjustment among titanates, 2) the τ_f compensation is proportional to the amount of SrT iO_3 in compensating mater ials, as well a s the thickness of the com pensating layer, and 3) th e most effective τ_f compensation is achieved when the co mpensating dielectric is integrated next to the SL. Using the effective dielectric con stant of a heterog eneous layered dielectric structure, results from Method of Mom entum (MoM) electrom agnetic simulations are consistent with the experimental observations.

ACKNOWLEDGMENTS

The authors thank Tom Chavez, Adrian Cas ias, Shelley W illiams, Adrian W agner and Dennis De Smet for help in sample fabrication and m easurement, and Dr Robe rt Grubbs and Dr Kevin Ewsuk for their critical review of the m anuscript. This work was supported by the Laboratory Directed Research and Developm ent program at Sandia National Laboratories, a m ulti-program laboratory managed and operated by Sandia Corporation, a wholly owned subsidiary of Lockheed Martin Corporation, for the U.S. De partment of Energy's National Nuclear Security Administration under contract DE-AC04-94AL85000.

CONTENTS

FIGURES

TABLES

NOMENCLATURE

α	Temperature coefficient of expansion
CTE	Temperature coefficient of expansion
CTO	$CaTiO_3$
CM	Co-Mill
CMA	Co-Mill powders with V-glass at 60 wt%
CMB	Co-Mill powders with V-glass at 55 wt%
CM	Co-Mill powders with V-glass at 49.5 wt%
ε	Dielectric constant
f_r	Resonant frequency
LTCC	Low temperature co-fired ceramics
MW	Microwave
RF	Radio frequency
SL	Strip-line
STO	$SrTiO_3$
TO	TiO_2
τ_c	Temperature coefficient of capacitance
τ_ε	Temperature coefficient of dielectric constant
τ_f	Temperature coefficient of resonant frequency

1. INTRODUCTION

A low τ_f, preferably close to 0 ppm/°C, is desirable to achieve resonator functions for radio and microwave frequency (RF and MW) applications that are stable to temperature variations. By using a low τ_f resonator the temperature compensation that requires additional mechanical [1] and electrical circuitry [2] can be eliminated. For filter applications, a low τ_f translates into an efficient use of frequency spectrum for maximum data capacity.

There are multiple approaches to achieve temperature stable resonator functions. One common engineering method of realizing a near zero τ_f is to form solid solutions of different dielectric ceramics that have opposite τ_f. Kell, Greenham and Olds [3] developed temperature-stable compositions in systems $Ca(Zr,Ti)O_3$ and $(Ba,Sr)(Zr,Ti)O_3$. Kucheiko *et al* [4] studied a $CaTiO_3$-$Ca(Al_{1/2}Ta_{1/2})O_3$ ceramic solid solution to identify a temperature stable composition for microwave applications. A general survey of microwave dielectrics, with an emphasis on temperature stability for resonators and filters, has been provided by Wersing [5]. In their review on microwave dielectric ceramics for mobile phone networks, Reaney and Iddles [6] summarized key factors that affect τ_f.

Other practice to realize a low τ_f is to form a hybrid layered structure incorporating alternating layers of opposite τ_f materials. Alford *et al.* [7] fabricated layered Al_2O_3-TiO_2 microwave dielectric resonators by sequential sintering of thick film TiO_2 (τ_f = +450 ppm/°C) on Al_2O_3 (τ_f = -60 ppm/°C) substrates. The τ_f of the resonators could be adjusted over a wide range, including 0 ppm/°C, by varying the thickness of TiO_2 layer. Li and Chen [8] adopted an approach of using adhesive-bonded $Ca(Mg_{1/3}Nb_{2/3})O_3$ and $Ba(Zn_{1/3}Nb_{1/3})O_3$ layered composite to form dielectric resonators. The τ_f could be tuned to 0 ppm/°C at a proper thickness ratio of the two constituents that possess opposite τ_f.

Low temperature cofired ceramic (LTCC) is a multilayer 3D packaging, interconnection and integration technology. An LTCC system refers to a base tape dielectric, typically a glass or glass-ceramic, and conductors (Au, Ag, Pt, etc) that are cofireable at temperatures 850 ~ 900 °C. Passive integration in LTCC, like embedded resistors and capacitors, is realized by cofiring specially engineered dielectric and resistive materials in paste or tape forms. In the past 20 years the largest growth of LTCC technology has occurred in wireless communications. The three dielectric material parameters most important to this application space include dielectric constant, ε, quality factor, Q (inverse of dielectric loss), and τ_f. For RF/MW LTCC circuits with embedded resonator functions, a near zero τ_f is necessary to fully utilize the communication bandwidth.

Although there are commercial LTCC dielectrics with low τ_f, e.g., Heraues CT2000 with τ_f < ±10ppm/°C, most of existing LTCC dielectrics have a τ_f in the range -50 to -80 ppm/°C. Figure 1 shows resonant frequency (f_r) versus temperature curves (normalized to f_r at 20 °C) for several main stream LTCC dielectrics along with τ_f data from this study. It is expected that, for integrated RF circuits using these LTCCs, the impact of τ_f will be reflected in the drift of the f_r of the embedded resonator over the device's operating temperatures. Often this results in a reduced working bandwidth, and an extra design limitation and/or a performance compromise.

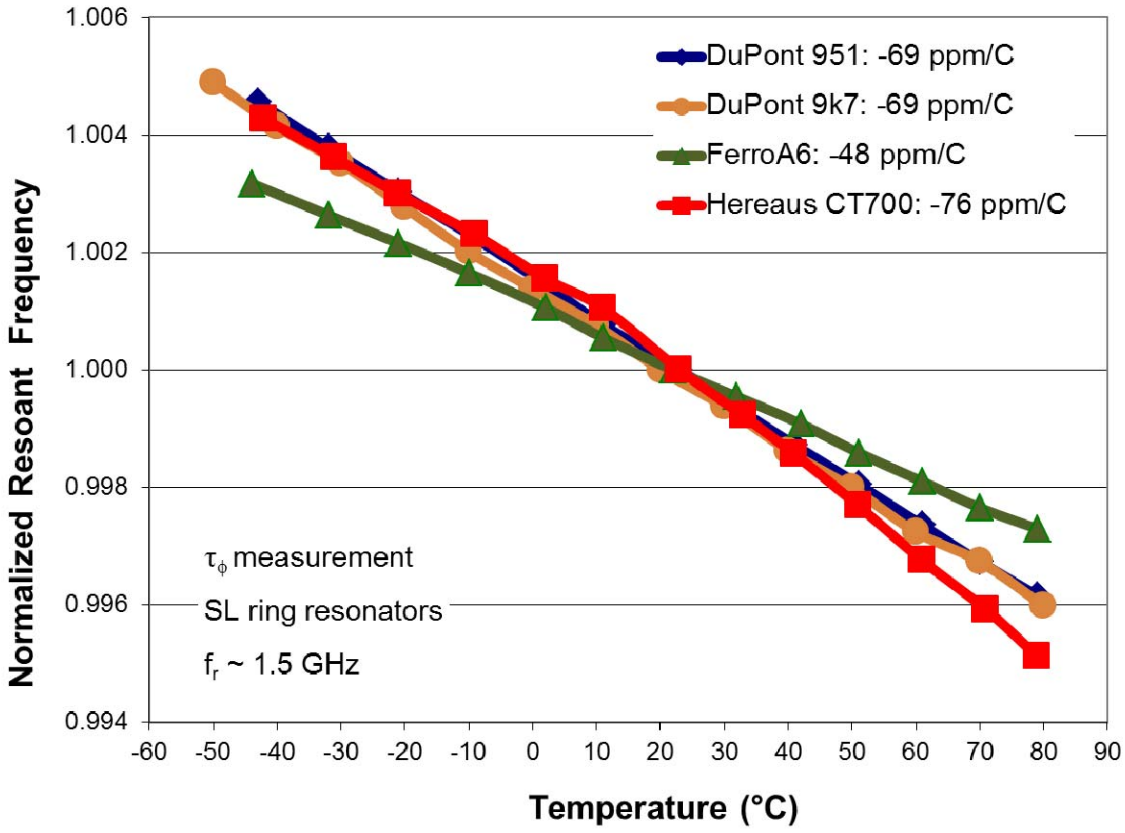

Figure 1. τ_f of several commercial LTCC base dielectrics from DuPont, Ferro and Hereaus. The resonant frequencies f_r (all ~ 1.5GHz) were collected from SL ring resonators from -50 to 80 °C, and normalized to f_r at 20 °C.

There have been many efforts to tune LTCC base dielectrics towards zero τ_f for MW and RF applications. Dai, Huang, and Wilcox [9] proposed using titanates (positive τ_f) to compensate for the negative τ_f of a glass-ceramic LTCC dielectric. Jantunen [10] investigated optimal compositions for $\tau_f < \pm 10$ ppm/°C in a LTCC consisting of zinc borosilicate glass mixed with $MgTiO_3$–$CaTiO_3$ ceramic fillers. Kapta, Inoue and Kato [11] achieved a τ_f of 1 ppm/°C in bismuth-based low fire dielectric ceramics. Choi, Park, and Park [12] developed middle-permittivity LTCC dielectrics with an adjustable τ_f.

The purpose of this study is to explore a novel approach to adjust the τ_f of a SL resonator in a multilayer LTCC structure by locally integrating a compensating dielectric with a τ_f opposite to that of the host LTCC dielectric. Upon successful implementation, this method would enable temperature compensation where only the resonator circuits reside in a compensating structure, which would avoid affecting other embedded functions where the implemention is unnecessary or undesirable. In principle, this method could be applied to any existing LTCC with a proper selection and development of cofireable compensating dielectrics. A major advantage of this approach is its inherent compatibility with the existing LTCC material systems, which enables the use of existing cofireable conductors and other functional materials, and circumvents the need to re-develop an entirely new LTCC materials system.

τ_f is a device parameter that can be expressed in basic material properties:

$$\tau_f = -\frac{1}{2}\tau_\varepsilon - \alpha \quad (1)$$

where τ_ε is the temperature coefficient of dielectric constant, and α the coefficient of thermal expansion (CTE). For LTCC dielectrics, α is typically between 4 ~ 10 ppm/°C, thus τ_ε dominates τ_f.

From eq. (1), it is clear that τ_f and τ_ε have opposite signs. To compensate for the negative τ_f of a LTCC, materials with a negative τ_ε and thus positive τ_f are necessary. Table 1 lists dielectric constant ε, τ_ε, and the normal sintering temperatures of candidate ceramics that could serve as compensating materials [13]. All three candidates are titanates, TiO_2, $CaTiO_3$ and $SrTiO_3$.

Table 1. Potential compensating materials.

Materials	Dielectric constant	τ_ε (ppm/°C)	Sintering Temp (°C)
TiO_2	110	-750	~ 1200
$CaTiO_3$	130	-1600	~ 1400
$SrTiO_3$	285	-2400	~ 1550

The key materials science challenges include synthesizing the τ_f compensating material and cofiring of the material with the existing LTCC system, for example, DuPont 951 LTCC. Evidence of both physical compatibility, measured by matched shrinkage, and chemical compatibility, characterized by material interdiffusion, is provided in this study. Multiple factors that affect τ_f adjustment, including the weight percentage of a titanate in the formulation, the thickness of the compensating layer, and the placement of τ_f compensating materials in multilayer LTCC, are examined throughout the investigation.

Analytic equations derived from the variational method with the transverse transmission-line technique [14-17] are presented to calculate the effective dielectric constant, ε_{eff}, of a SL in a symmetric multilayer LTCC structure. The Method of Momentum (MoM) simulated resonant frequency (f_r) of the SL resonators at temperatures between -50 °C to 80 °C is obtained based on temperature related dielectric constants of the τ_f adjusters and LTCC. Using this method, the thickness and configuration of STO can be optimized for the best temperature compensation. The simulated τ_f was also compared to experimental data for model validation.

2. EXPERIEMNTS

2.1. Design of τ_f Compensating Materials

DuPont 951 LTCC GreenTape™, a widely used LTCC system in the industry over the last 20 years, was selected as the host dielectric system for the localized τ_f compensation experiments. The 951 LTCC is a tape that is cast and dried from a slurry of a mixture of glass-ceramic (LTCC glass plus Al_2O_3 ceramic filler) dispersed in an organic vehicle. To match the 951 LTCC chemistry, an attempt was made to formulate the τ_f compensating materials the same way, i. e., making the material a mixture of a LTCC glass and ceramic fillers. Al_2O_3 was used as the filler for the base compensating material. A series of compensating materials were formulated by replacing part of the Al_2O_3 in the composition with a titanate as the τ_f adjuster. The main factors considered were the chemical constituents of the glass, and the glass softening point, T_g, which correlates closely to the onset temperature of shrinkage of the compensating material. Ideally, the onset temperature of shrinkage and the rate of shrinkage of the compensating materials would match those of 951 LTCC. In addition, no or minimal interaction between the compensating material and the LTCC was also desirable. One specific LTCC glass, designated as V-glass, was selected for this study after an evaluation of several commercial LTCC glasses.

2.1.1. Formulation of τ_f compensating materials

Table 2 details the formulations of the compensating materials used in this study. CM stands for co-milled powders; A, B and C refer to weight percentage of V-glass at 60, 55 and 49.5 wt%; TO = TiO_2, CTO = $CaTiO_3$ and STO = $SrTiO_3$; and the number represents weight percentage of an appropriate titanate that replaces Al_2O_3 as the filler material. Most of the compositions studies were CMB formulation where the base formulation is 55 wt% V-glass + 45 wt% Al_2O_3 without the addition of a titanate. There were three objectives to formulate these compositions: 1) to study the effect of the type of titanates, 2) to study the effect of the amount of a titanate, and 3) to study the effect of the LTCC glass to ceramic filler ratio on the τ_f adjustment on a SL resonator.

Table 2. Formulation of compensating materials (CM = Co-mill).

Composition	V-glass (wt%)	Al_2O_3 (wt%)	TiO_2 (wt%)	$CaTiO_3$ (wt%)	$SrTiO_3$ (wt%)	Total wt%
CMB base	55	45				100
CMB TO15	55	30	15			100
CMB TO30	55	15	30			100
CMB CTO10	55	35		10		100
CMB CTO20	55	25		20		100
CMB STO10	55	35			10	100
CMB STO20	55	25			20	100
CMB STO25	55	20			25	100
CMB STO30	55	15			30	100
CMA STO20	60	20			20	100
CMC STO20	49.5	30.5			20	100

2.1.2. Synthesis of τ_f compensating materials

The mixture of V-glass, Al_2O_3 and titanate was co-milled to a median particle size 2.0 to 2.2 μm using Al_2O_3 media. Pellets with a diameter 12.5 mm and a thickness 1 mm were formed by dry pressing co-milled powder granulated with organic binder. A 2-step pressing process was used for pellet compaction, which involved uniaxial pressing at 43.5 MPa followed by isostatic pressing at 206.8 MPa. The pellets were sintered at 850 °C for 30 min in air. Density of all sintered materials was measured using Archimedes method. Electrodes were deposited by sputtering Au on polished sintered pellets for measurement of dielectric properties.

Pastes of selected compensating materials were made using an organic vehicle, ESL441, combined with the thinner, ESL401, (both from Electro-Science Labs) using a 3-roll mill. These pastes were screen printed on green LTCC tapes to form temperature compensation layers for SL ring resonators.

2.2. SL Resonator Panels

2.2.1. Construction of panels

Standard 254 μm thick DuPont 951 LTCC tapes were used throughout this study. The conductors used include DuPont 5738 Au for the via fill, 5734 Au for the internal conductors, and 6143 Ag/Pd for the post-fired external metallization. SL ring resonators having a designed base resonance of 1.5 GHz were fabricated in 4 layer 951 panels. Figure 2 shows the LTCC tapes, before and after sintering, of a resonator layer with a printed CMB STO20 layer between the ring resonator and the 951 dielectric. The line width of the Au ring is 0.2 mm. The width of the printed CMB STO20 is 4 mm. All panels were laminated using a standard process that included 20.7 MPa isostatic pressing at 70°C for 10 minutes. Panels were sintered at 850 °C for 30 min in air on Al_2O_3 setters. Sub-miniature version A (SMA) edge connectors were soldered to resonator panels to access the embedded ring resonator for f_r measurements. Figure 3 shows green, sintered and finished SL resonator panels with the embedded CMB STO20.

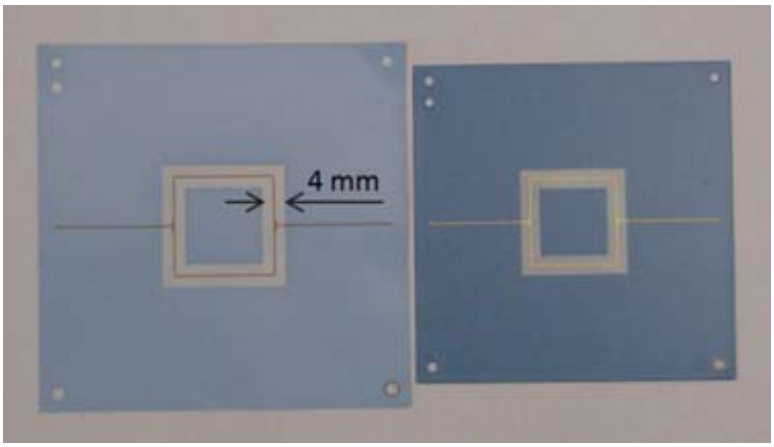

Figure 2. Au ring resonator and feed lines on 75×75 mm green (left) and sintered (right) 951 tape with a printed STO layer in between.

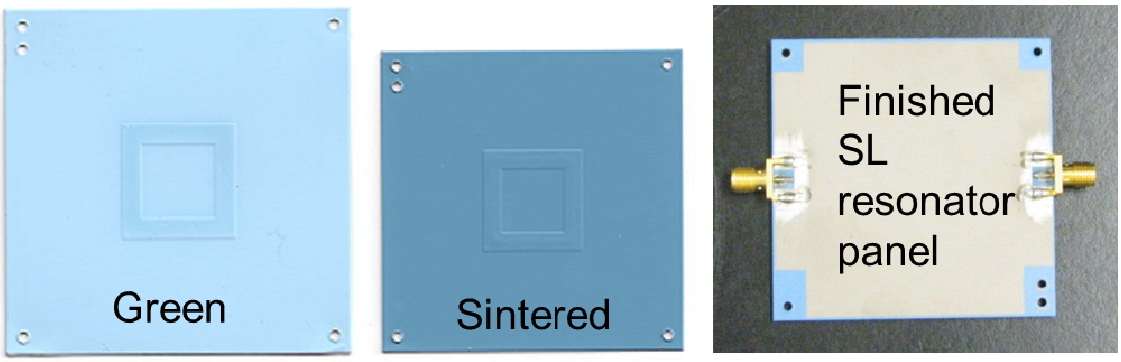

Figure 3. Green, sintered, and finished SL resonator panels.

2.2.2. Incorporation of τ_f adjusters in resonator panels

The screen printed τ_f adjusters are in a square ring pattern. The square Au ring is positioned at the center of the 4 mm wide τ_f adjusters. Using an 80 μm thick 325 mesh screen, a typical thickness of the sintered τ_f adjusters layer is 18 ~ 20 μm from a single print, and 35 ~ 40 μm from a double print using a print-dry-print process. Extra 951 tapes with the same printed τ_f adjusters were fabricated and sintered along with the resonator panels for measurement of the paste thickness using a Cobra laser profilometer. The measurement was taken after the paste was dried in an oven, as well as after the tapes were sintered. These tapes were also cross sectioned to examine the actual thickness of the pastes by optical microscopy. Inspection of the τ_f adjuster layer showed a variation in thickness, typically ± 3 μm, over the targeted thicknesses.

2.3. Characterization

2.3.1. τ_f compensating materials

2.3.1.1. Sintering behavior

Shrinkage data for the compensating material, in the form of a cylinder of diameter of 6.25 mm and thickness of 5 mm, and the 951 dielectric, in the form of a 5x5 mm stack of 20 layer tapes, were collected in air using a Netzsch DIL 402 dilatometer.

2.3.1.2. Dielectric properties

The capacitance of the compensating materials was measured on sintered pellets using a HP4194A impedance analyzer at 1 MHz over a temperature range -50 °C to 80 °C. The capacitance of the 951 dielectric was measured on 12.75x12.75x0.405 mm coupons with sputtered Au for electrode material.

2.3.1.3. Microstructure

The crystalline phases in the τ_f compensating materials were identified by X-ray diffraction (XRD) using a Siemens D500 diffractometer employing a sealed tube X-ray source (Cu K α

radiation), fixed slits, a diffr acted-beam graphite m onochromator, and a scintillation detector . Typical scans were perfor med from 5 to 80 degrees 2 θ using a 0.04º step size at 2 sec/step. Sintered microstructure was exa mined using a Zeiss Supra 55VP field em ission scanning electron microscope (SEM), where the Energy Dispersive Spectroscopy (EDS) was perform ed with a Bruker Quad SDD detector and Bruker Esprit software.

2.3.2. SL resonator panels

2.3.2.1. Measurement of f_r

The SL resonators were placed inside a temperature chamber and characterized using an Agilent E5062A network analyzer from -50 °C to 80 °C. Figure 4 shows the experi mental setup used to measure the S-param eters of a SL LTCC resona tor. The panel was h eld by the m easurement cables via the SMA connectors with a K-type ther mocouple attached to the surface. Prior to conducting the measurement, a standard calibration was perf ormed on both ports of the E5062A using an A gilent calibration kit under open/sh ort/load/through conditions. The S-param eters, S11, S12, S21 and S22, were collected over a 0. 3 GHz frequency span centered at ~1.5 GHz at each temperature. The f_r was obtained as the minim um frequency of th e reflection coefficient (S11) of the ring resonator. The τ_f of a resonator was calculated using the following equation,

— —) (2)

where f_{ro} is the resonant frequency at 20 °C, Δf_r is the change of resonant frequency over -50 to 80°C, and ΔT equals to 130 °C.

Figure 4. f_r test setup, and the mounting of a SL resonator panel.

2.3.2.2. Integrated STO layers

Cross sections of some sintered SL resonator panels were made to inspect the cofired multilayer structure. The cross sections were exam ined by optical m icroscopy to m easure the actual thickness of the compensating material. The same cross sections were also analyzed by SEM for possible interfacial reactions between the 951 LTCC and the compensating material.

3. CALCULATION OF EFFECTIVE DIELECTRIC CONSTANT AND SIMULATION OF RESONANT FREQUENCY

An effective dielectric constant of a SL is

(3)

where C is the total SL capacitance, and C_o is the total SL capacitance in air. Using a variational method [13], C can be expressed as

(4)

where

(5)

is the Fourier transform of the charge density distribution f(x), β is the propagation constant, Q is the total SL charge, w is the strip width, and Y is the admittance from the SL.

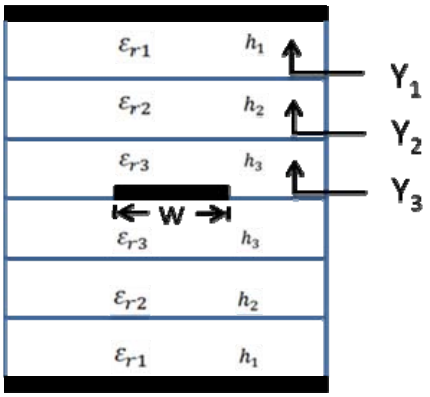

Figure 5. Admittance from dielectric interfaces.

A schematic cross section of a four tape LTCC structure with embedded SL and τ_f compensating materials is illustrated in Figure 5. The SL is sandwiched between symmetrical three layers of dielectrics, with a dielectric constant of ε_{r1}, ε_{r2} and ε_{r3}, and a corresponding layer thickness of h_1, h_2 and h_3. The surfaces are designated as the ground planes.

Y_1, Y_2, Y_3 are the transverse transmission line admittances between the dielectric interfaces and the ground plane. The admittance can be expressed for each successive layer [15, 16] as,

(6)

$$Y_2 = \varepsilon_o \varepsilon_{r2} \frac{Y_1 + \varepsilon_o \varepsilon_{r2} tanh(\beta h_2)}{\varepsilon_o \varepsilon_{r2} + Y_1 tanh(\beta h_2)} \quad (7)$$

$$Y_3 = \varepsilon_o \varepsilon_{r3} \frac{Y_2 + \varepsilon_o \varepsilon_{r3} tanh(\beta h_3)}{\varepsilon_o \varepsilon_{r3} + Y_2 tanh(\beta h_3)} \quad (8)$$

At the charge plane of the SL, the total transverse admittance $Y = 2Y_3$,

$$Y = 2\varepsilon_o \varepsilon_{r3} \frac{Y_2 + \varepsilon_o \varepsilon_{r3} tanh(\beta h_3)}{\varepsilon_o \varepsilon_{r3} + Y_2 tanh(\beta h_3)} \quad (9)$$

For an air filled SL, the total capacitance is

$$\frac{1}{C_o} = \frac{1}{\pi} \int_0^\infty \frac{\left[\frac{\tilde{f}(\beta)}{Q}\right]^2}{\beta} \frac{1}{Y_o} d\beta \quad (10)$$

The transverse transmission line admittance reduces to

$$Y_{30} = \varepsilon_o coth[\beta(h_1 + h_2 + h_3)] \quad (11)$$

The total transverse transmission line admittance at the **c**harge plane of a SL is then,

$$Y_o = 2Y_{30} = 2\varepsilon_o coth[\beta(h_1 + h_2 + h_3)] \quad (12)$$

Once all th ree dielectrics were charact erized over a tem perature range, the ε_{eff} is calculated numerically at each temperature u sing MatLab. The f $_r$ of the SL ring re sonator at a given temperature was simulated using ε_{eff} and the Method of Mom entum. Finally, a curve of f_r versus temperature was constructed, from which the τ_f was calculated using equation (2).

4. RESULTS AND DISCUSSION

4.1. τ_f Compensating Materials

4.1.1. Dielectric properties

Table 3 shows the dielectric constant, ε, of each composition at -50 ºC, -20 ºC, 0 ºC, 20 ºC, 50 ºC and 80 ºC. The sintered density of compensating material, the ε at 20 ºC, the τ_ε of compensating material, and an estimated τ_f (assuming a $\alpha \sim 6$ ppm/ºC for all the STO compositions, and using equation (2)) are listed in Table 4 for each composition. Both CMB TO10 and CMB TO30 showed a lack of adequate densification, so these compositions were dropped from further study. Note that the estimated τ_f of 951 LTCC is -59 ppm /°C, lower than the -69 ppm /°C (Figure 1) measured for a SL resonator in a 951 panel. The source of the discrepancy was unclear but may partially result from the measurement errors in sample dimension, and the determination of ε.

Table 3. Dielectric constant of τ_f compensating materials from -50 ºC to 80 ºC.

Temp (°C)	951 LTCC	CMB Base	CMB_ CTO10	CMB_ CTO20	CMB_ STO10	CMB_ STO20	CMB_ STO25	CMB_ STO30	CMA_ STO20	CMC_ STO20
-50	7.82	7.70	9.69	12.09	9.58	12.49	14.34	16.46	12.22	12.49
-20	7.84	7.74	9.70	12.04	9.57	12.35	14.12	16.10	12.09	12.37
0	7.86	7.76	9.72	12.02	9.57	12.28	13.99	15.92	12.02	12.32
20	7.88	7.79	9.73	12.00	9.57	12.22	13.88	15.76	11.96	12.27
50	7.90	7.83	9.76	11.98	9.57	12.15	13.75	15.57	11.89	12.21
80	7.93	7.89	9.80	12.00	9.59	12.10	13.66	15.39	11.85	12.18

Table 4. Density, room temperature dielectric constant ε, τ_ε, and estimated τ_f of compensating materials.

Sample	Archimedes bulk density (g/cc)	ε (1 MHz at RT)	τ_ε (ppm/ºC)	Estimated τ_f (ppm/°C)
951 LTCC	3.10	7.88	112	-59
CMB base	3.19	7.79	190	-99
CMB TO10	N/A			
CMB TO30	2.77			
CMB CTO10	3.20	9.72	83	-45
CMB CTO20	3.15	12.0	-58	26
CMB STO10	3.21	9.57	10	-9
CMB STO20	3.30	12.22	-240	117
CMB STO25	3.31	13.88	-379	186
CMB STO30	3.35	15.76	-525	259
CMA STO20	3.23	11.96	-241	117
CMC STO20	3.35	12.27	-192	93

It should be noted that the addition of titanates to the base V-glass + Al_2O_3 glass ceramics does result in higher dielectric constants. The higher dielectric constant is expected to decrease the f_r of a SL resonator when the cofired compensating material is integrated into the LTCC.

4.1.2. Chemistry

XRD patterns of the base dielectric and the two $SrTiO_3$ modified compensating materials CMB STO10 and CMB STO20 are shown in Figure 6. It is evident that Al_2O_3 is the main crystalline phase in the base dielectric, with the amorphous background between 2 θ value of 20 to 35 degrees representing the V-glass. There is also a minor amount of anorthite, $CaAl_2Si_2O_8$, in the base dielectric, presumably derived from the reaction between Al_2O_3 and the V-glass. For CMB STO10, the major crystalline phases are Al_2O_3 and $SrTiO_3$, with a minor anorthite phase. As expected in CMB STO20, the $SrTiO_3$ peaks grow much stronger relative to the Al_2O_3 peaks. The anorthite phase nearly disappears in CMB STO 20, indicating a suppression of the interaction between Al_2O_3 and the V-glass. For both STO10 and STO20, there is no indication of compounds forming from a glass-$SrTiO_3$ interaction. This absence of interaction is beneficial to the sintering of $SrTiO_3$ modified compensating materials since the densification is a relatively simple viscous sintering of a glass-ceramic body. It has been shown that crystallization during sintering of a glass-ceramic composite, either self-derived from the glass, or reaction-derived from glass-ceramic interaction, can significantly impede the densification process [18, 19].

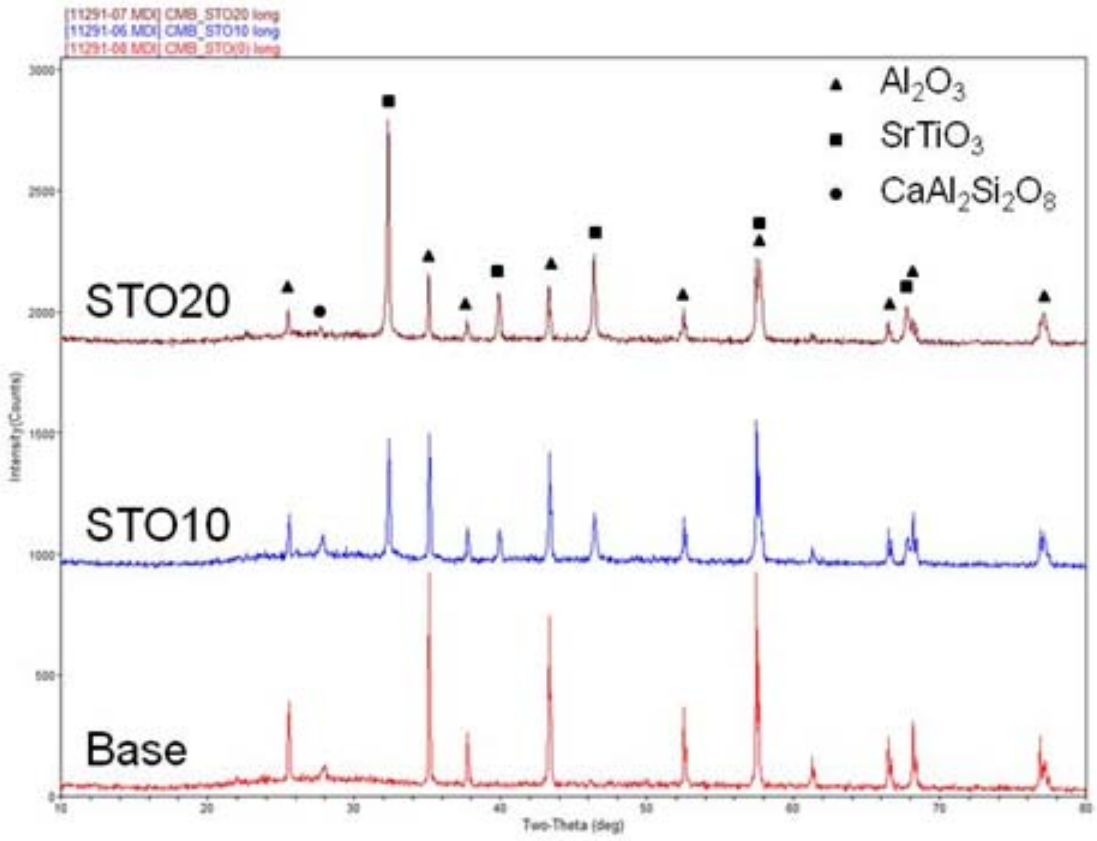

Figure 6. XRD of sintered compensating materials, STO10 and STO20, compared to the base dielectric.

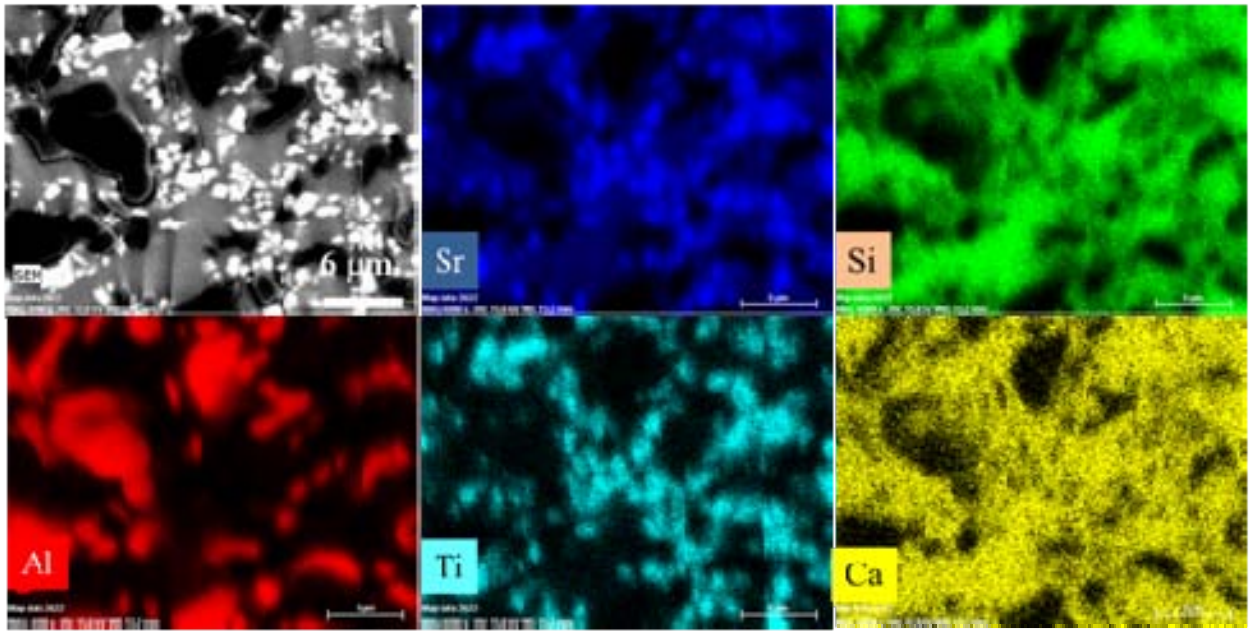

Figure 7. SEM image and element mapping of STO20.

The lack of interaction between the ceramic particles, Al_2O_3 and $SrTiO_3$, and the V-glass is further validated by SEM observations. Figure 7 shows a SEM image of a polished CMB STO20 surface along with elemental maps of Al, Sr, Ti, Si and Ca. The microstructure has three distinct phases, the fine $SrTiO_3$ particles (in white), the relatively coarse Al_2O_3 particles (in black), and a continuous glass phase (in grey). The clean boundaries of $SrTiO_3$ and Al_2O_3 particles suggest that there is no, or a minimal if any, reaction between these ceramic particles and the surrounding V-glass. There is also minimum amount of porosity in the microstructure, indicating a highly densified glass-ceramic body. This result is consistent with the measure density of 3.30 g/cm^3 for CMB STO20 (see Table 4).

4.2. τ_f Compensating Materials and 951 LTCC

There are several progressive levels of requirements to successfully synthesis τ_f compensating materials: 1) the materials should have large enough τ_f that is opposite to that of 951 LTCC for effective compensation, 2) the materials should have a shrinkage and shrinkage rate that closely match to the 951 LTCC to avoid warping of the cofired structures, and 3) there should be either least, or ideally no, chemical reactions or inter-diffusion between the τ_f compensating materials and the 951 LTCC to preserve the τ_f compensation properties.

4.2.1. Physical compatibility

Figure 8 plots the shrinkage curves of CMB STO20 and 951 in the Z-direction (through the thickness of the tape) for a heating rate of 5 °C/m in from 500 to 850 °C. The onset temperature for shrinkage of CMB STO20, measured from a shrinkage-versus-temperature plot, is 741 °C. Among all of the LTCC glasses evaluated, the onset temperature of V-glass based STO

composition represents the closest match to the onset temperature of 766 °C for the 951 LTCC. In addition, the shrinkage rates of the two materials, represented by the slopes of the shrinkage curves during the temperature ramp up period, track closely to each other. The proximity of these onset temperatures and shrinkage rates provides a solid physical basis for successfully cofiring CMB STO20 with 951 LTCC.

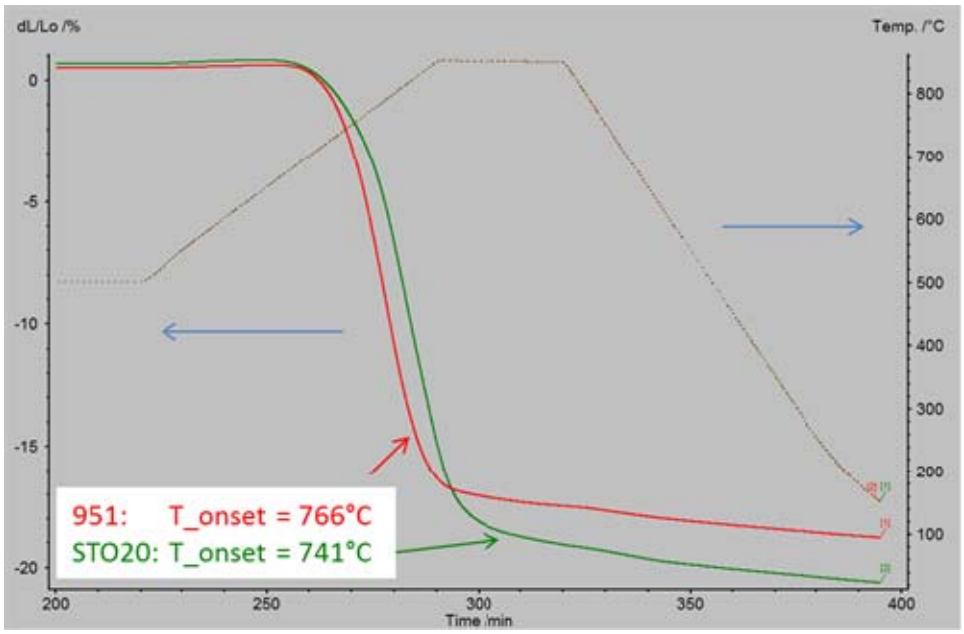

Figure 8. Shrinkage curves and onset temperatures of CMB STO20 and 951 LTCC.

4.2.2. Chemical compatibility

To verify the cofireability of CMB STO20 with the 951 tape, a square ring pattern of STO20 paste was screen printed onto a 75x75 mm 951 single tape and sintered using a normal profile (similar to Figure 2 without the Au conductor). Figure 9a shows an optical image of a fractured cross section of the cofired structure. No deformation in either the 951 or the CMB STO20 is visible, indicating well-matched sintering. A close look at the STO20-951 interface by SEM is also presented in Figure 9b. A relatively clean interface exists between the two cofired materials, suggesting no or minimal chemical interaction and/or inter-diffusion between the two materials.

Figure 9. a) Optical cross section of sintered CMB STO20 on 951, and b) a SEM cross section of the interface between the CMB STO20 and the 951 LTCC.

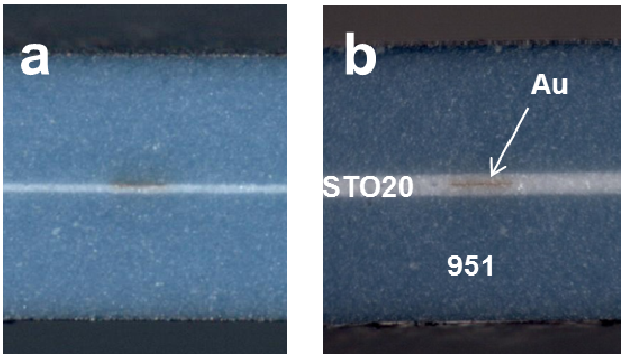

Figure 10. Embedded CMB STO20 in a 4 layer 951 LTCC, a) one side, and b) both sides of the Au conductor.

To further analyze the interfaces of embedded τ_f compensating material in the 951 LTCC, SL resonator panels with CMB STO20 were cross sectioned for both optical and SEM examination. Figure 10 is an optical image of CMB STO20 cofired in a 4 layer 951 LTCC shown, a) one side, and b) both sides of the Au conductor. The hybrid multilayer panel confired nicely without any noticeable warping of the structure or delamination at the interfaces.

The cross section was further examined by SEM. Figures 11a and 11b show an image of a Au line embedded in the CMB STO20 dielectric, and the corresponding Si map, respectively. It appears that the Au reaches nearly a full sintered density without noticeable glass penetration from the surrounding CMB STO20. The small Si inclusion inside the Au in Figure 11b (pointed at with an arrow) may be attributed to the minor amount of glass frit in the 5734 Au paste used to match the shrinkage to that of the 951 LTCC.

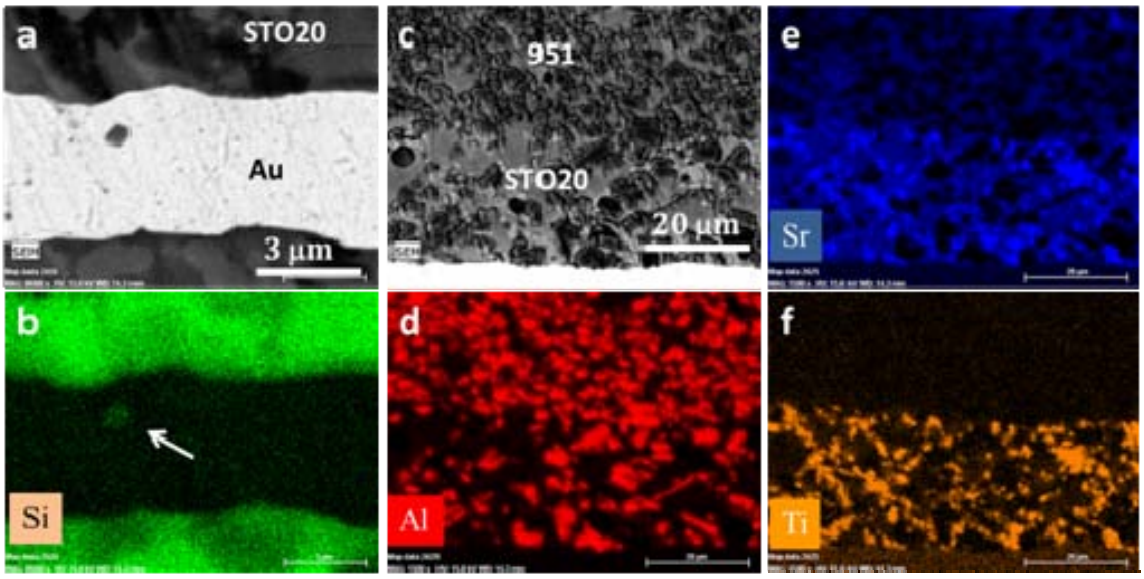

Figure 11. a) SEM cross-section image of cofired STO20 dielectric and Au resonator line; b) mapping of Si element in a); c) SEM image of embedded STO20 in 951 LTCC. The correspondent element maps for Al, Sr and Ti are shown in d), e) and f).

Figure 11c shows a well-defined boundary between the 951 and the CMB STO20 in the cofired structure despite the obvious difference in the volume density and the size of Al_2O_3 particles in the two materials observed in figure 11d. The boundary is very distinct in the Ti mapping shown in Figure 11f, where Ti only exists in the CMB STO20 but not in the 951. Again the SEM analysis indicates that CMB STO20 can be cofired with 951 LTCC without noticeable inter-diffusion between the two.

4.3. τ_f Compensation

In this section the effects of temperature compensation are examined from different perspectives. Initially, the estimated τ_f of each compensating material was used to judge whether it provided adequate temperature compensation. Then, SL resonators panels using selected τ_f compensating materials were built at different layer thicknesses and configurations to study the effectiveness of the temperature compensation.

4.3.1. Effect of titanates

Figure 12 shows the normalized ε, scaled to the ε value at 20 °C, for τ_f compensating materials over the temperature range -50 °C to 80 °C. The estimated τ_f values from τ_ε data are listed in the legend (from Table 4). The plot visualizes the change in the slope as the amount of a titanate increases in the compositions. Obviously, only the compositions that have an opposite slope to that of 951 LTCC can be used to compensate the temperature effect.

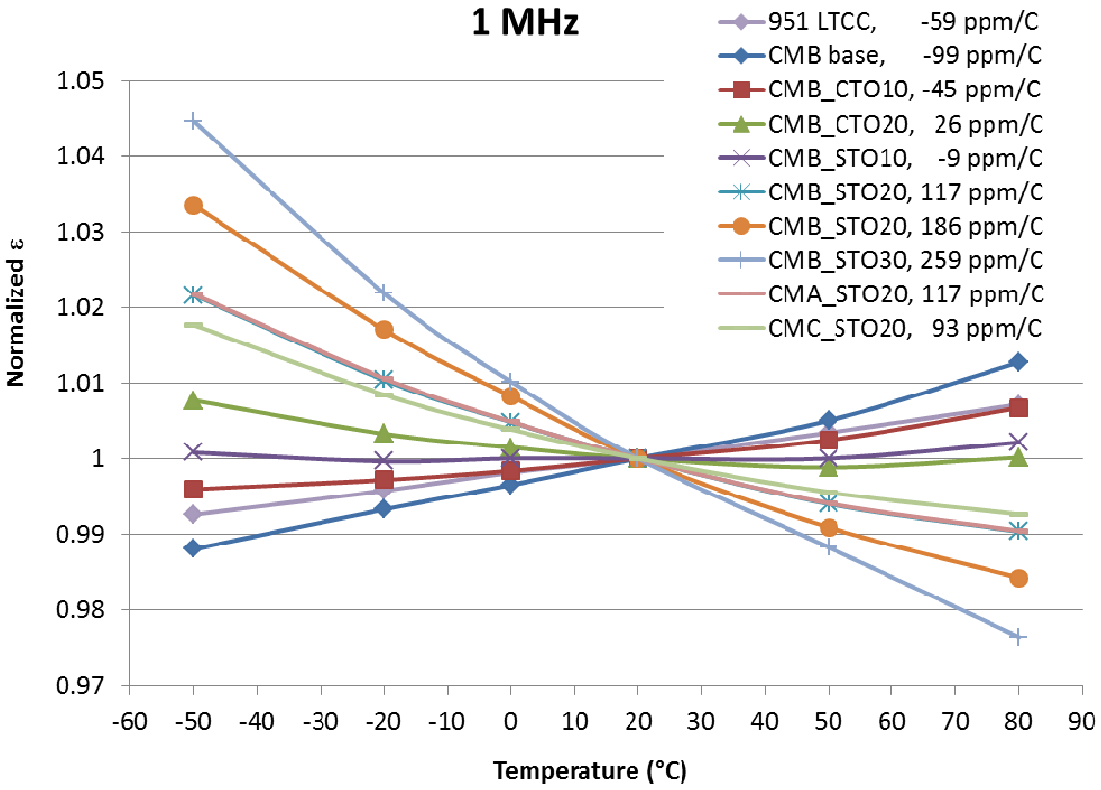

Figure 12. Tempeature dependence of normalized ε of compensating materials.

The CMB base dielectric has a τ_ε of 190 ppm /°C, and a τ_f of -99 ppm /°C. So, without the addition of titanates, the base dielectric has a higher τ_f than the 951 LTCC. With the addition of 10 wt% of titanates, the CTO10 and STO10 still show positive τ_ε, and thus negative τ_f. Obviously, the polarity of τ_f of these two compositions is the same as that of the 951 LTCC. These compositions are not expected to adjust the τ_f towards zero and were eliminated from further investigation. With a higher weight percentage of CTO and STO, the CMB CTO20 and CMB STO20 reach a τ_f of 25.5 ppm/°C and 117 ppm/°C, respectively. Considering that the 951 LTCC has a τ_f of -69 ppm/°C, the CMB STO20 is expected to be more effective for τ_f compensation, and was thus down-selected for cofiring studies, microstructure analysis, and for the fabrication of proof-of-concept SL ring resonators.

The estimated τ_f of CMB STO25 and CMB STO30 at 180 ppm /°C and 259 ppm /°C, respectively, further increases from 117 ppm/°C for CMB STO20. Thus, it is expected that these two compositions could adjust the τ_f much more effectively than CMB STO20. Both compositions were selected to be incorporated in SL resonator panels.

The ε and estimated τ_f of CMA STO20 and CMC STO20 are close to those of CMB STO20 (Table 3 and 4), suggesting that the effect on τ_f compensation from the amount of V-glass is much less significant compared to the kind and the amount of a titanate. Thus similar τ_f adjustments are expected from these three compensating formulations.

4.3.2. Effect of glass and STO content

SL resonator panels were fabricated using STO compositions with a layer thickness of approximately 20 μm. Table 5 lists τ_f data for two separate comparisons: 1) at a fixed STO20 concentration to assess the effect of glass to filler weight ratio from CMA of 60/40, CMB of 55/45 to CMC of 49.5/50.5, and 2) at a fixed CMB of 55 wt% glass to assess the effect of STO content of 20, 25 and 30 wt%.

The glass to filler ratio from CMA to CMB has a minimum impact on the temperature stability, as the τ_f of the SL resonators are -29.5 and -28.8 ppm/°C, respectively. However the τ_f of CMC STO20 is -41.3 ppm/°C, consistent with the estimated higher τ_f of the CMC STO20 composition in Figure 13.

Table 5. τ_f data for SL resonators using different STO compositions and a layer thickness of approximately 20 μm.

STO compositions in SL resonator	τ_f (ppm/°C)
CMA STO20	-29.5
CMB STO20	-28.8
CMB STO25	-13.4
CMB STO30	0.5
CMC STO20	-41.3

The temperature stability of the resonator improves as the wt% of STO increases. The CMB STO20 with 20 wt% STO in the composition reduces the τ_f to -28.8 ppm/°C from -69 ppm/°C of the uncompensated 951 LTCC. In CMB STO25, the τ_f is further reduced to -13.4 ppm/°C. A near zero τ_f of 0.5 ppm/°C is achieved in CMB STO30. It is clear that the content of STO plays an important role in temperature compensation, and the most effective compensating material is the CMB STO30 which has the highest STO wt% in this study.

4.3.3. Effect of STO layer thickness

SL resonators made using the print-dry-print deposition of STO layers of approximately 40 μm thick were also fabricated to examine the effect of STO thickness. Table 6 displays τ_f data for resonators made using 20 and 40 μm CMB STO20, CMB STO25 and CMB STO30 layers. For CMB STO20, the doubling of thickness from 20 to 40 μm reduces the τ_f of -28.8 to a near zero 1.9 ppm/°C. The same doubling in thickness of CMB STO25, however, overcorrects the τ_f from -13.4 to 41.2 ppm /°C. It is reasonable to assume that a true zero τ_f could be achieved with a CMB STO25 thickness between 20 and 40 μm. The overcorrection of τ_f for CMB STO30 is even more pronounced, as evidenced by a τ_f of 60.8 ppm/°C with a 40 μm thick CMB STO30 versus a τ_f of 0.5 ppm/°C at 20 μm.

Table 6. τ_f data of SL resonator panels at STO thickness of 20 and 40 μm.

STO compositions in SL resonator	τ_f (ppm/°C)	
	20 μm	40 μm
CMB STO20	-28.8	1.9
CMB STO25	-13.4	41.2
CMB STO30	0.5	60.8

Overall the thickness of the STO layer has a significant effect on the τ_f of the resonators. A thicker STO layer results in more temperature compensation. Data in Table 6 suggest that a zero τ_f is readily achievable with a proper combination of STO composition and the layer thickness. The results bring in design flexibility and paths for process optimization. For example, if a minimum amount of compensating material is needed in a LTCC multilayer structure, then the CBM STO30 is the choice. On the other hand, if better tolerance and process consistency can be achieved using a thicker STO layer then the CMB STO20 might be used in a LTCC structure.

4.3.4. Effect of STO configuration

Three symmetrical configurations of STO placement, as shown in Figure 13, were examined in this study: 1) STO layers printed next to the Au resonator ring, 2) STO layers printed 1 LTCC tape layer away from the Au ring, and 3) STO layers printed 2 LTCC tape alyers away from the Au ring, i.e., just under the top and bottom ground planes. Table 7 lists the actual stack-up of dielectric layers for each STO configuration in Figure 5 for the ε_{eff} calculation.

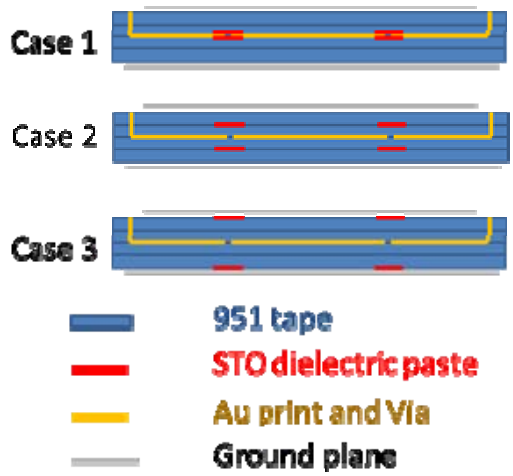

Figure 13. Three configurations of printed STO layers examined.

Table 7. Dielectric layer in the three configurations used in this study.

Configuration	ε_{r1}	ε_{r2}	ε_{r3}
Case 1	STO	951	951
Case 2	951	STO	951
Case 3	951	951	STO

The τ_f data for multiple SL resonator panels incorporating CMB STO20 and CMB STO30 are shown in Table 8. 20 and 40 μm STO layers were printed on to different LTCC tapes according to Figure 13. Resonators with 40 μm CMB STO20 in cases 2 and 3 were not fabricated and measured, since it is clear from Table 8 that even resonators using 40 μm CMB STO30 are far from reaching a zero τ_f.

It becomes evident that, only in case 1, where the STO layers are placed next to the SL resonator, can a zero τ_f be achieved using localized STO compensation. In case 3, the τ_f for a 20 μm thick layer of either STO20 or STO30 is very close to the uncompensated τ_f = -69 ppm/°C of the 951 LTCC. There is essentially no τ_f adjustment. At a layer thickness 40 μm, the τ_f of CMB STO30 drops only to – 62.3 ppm /°C. Moving the STO layers closer to SL in case 2 does reduce τ_f slightly, but the τ_f compensation is very limited, and far from reaching a true 0 ppm/°C. Placing the compensating STO materials next to the SL resonator appears to be the most effective, and may be the only practical, way to achieve τ_f compensation.

Table 8. τ_f of SL resonators with different STO layer thicknesses and configurations.

Composition	STO thickness (μm)	τ_f (ppm/°C)		
		Case 1	Case 2	Case 3
CMB STO20	20	-28.8	-67.5	-71.2
	40	1.9		
CMB STO30	20	0.5	-61.7	-69.3
	40	60.8	-54.8	-62.3

4.4. Simulated τ_f Results

4.4.1. Effect of STO composition and thickness

For case 1 where the STO is placed next to the SL, Figure 14 shows calculated ε_{eff} as a function of temperature for CMB STO20 and CMB STO30 at a thicknesses from 5 μm to 50 μm. As the STO20 layer becomes thicker, the ε_{eff} increases accordingly. At the same time, the slope of ε_{eff} changes from positive at 5 μm to nearly flat at 50 μm. Larger changes in ε_{eff} over the same thickness range are seen for CMB STO30 since the CMB STO30 has a higher ε to begin with. One important distinction for the ε_{eff} of CMB STO30 is the change of the slope. Similar to CMB STO20, the slope of ε_{eff} starts as negative at 5 μm layer thickness, but ends as positive at 50 μm. The ε_{eff} is nearly flat over temperature for a 20 μm layer thickness.

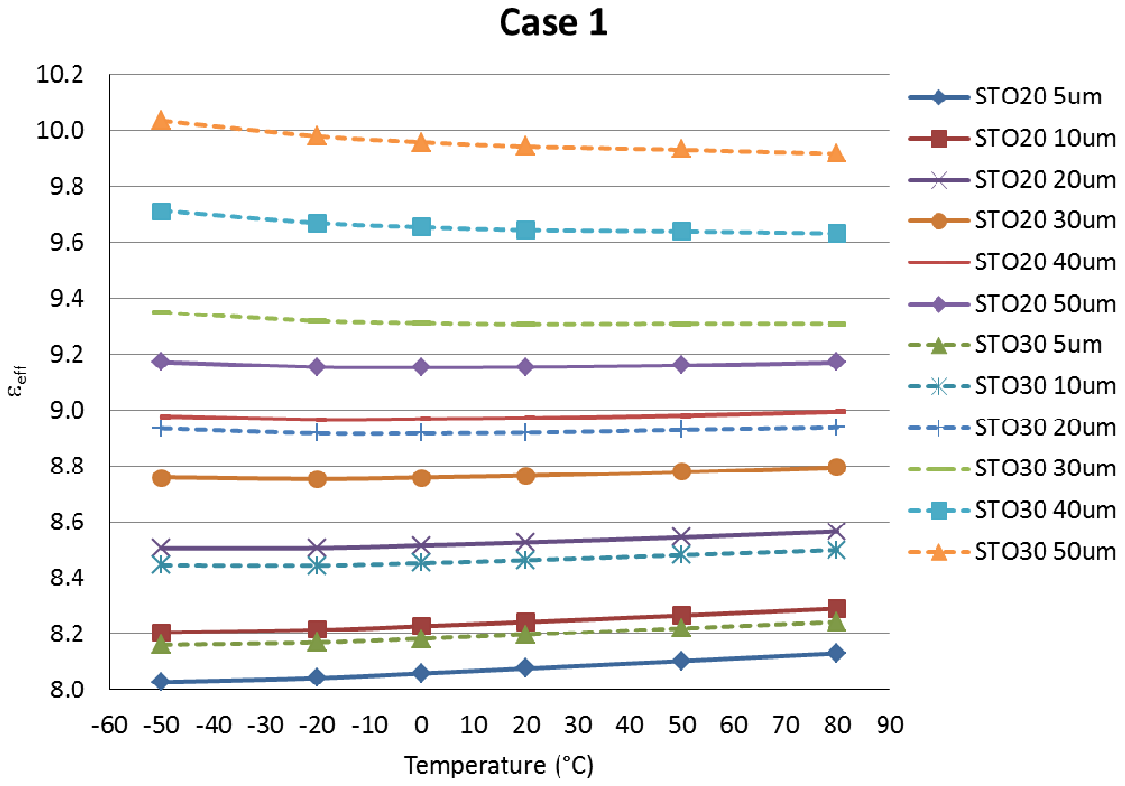

Figure 14. ε_{eff} of SL as a function of temperature and STO layer thicknesses from 5 to 50 μm.

Figure 15 plots the simulated f_r versus temperature for the same STOs from 5 μm to 50 μm thick, with the corresponding τ_f values (slope of the $f_r \sim T$ curves) shown in the legend. The simulated f_r reflects the changes in ε_{eff}: f_r decreases as ε_{eff} increase, as f_r correlates to ε by $f_r \sim 1/\sqrt{\varepsilon}$. For CMB STO20, τ_f decreases as the layer becomes thicker. At a thickness 20 μm the simulated τ_f is equal to -26.9 ppm/°C, which is very close to the -28.8 ppm/°C measured from the SL resonator (Table 6). The simulated τ_f reaches 0.5 ppm/°C at a thickness 50 μm, while the measured τ_f is 1.9 ppm/°C at a thickness 40 μm, suggesting that the simulation might underestimate the τ_f when a STO layer becomes thicker.

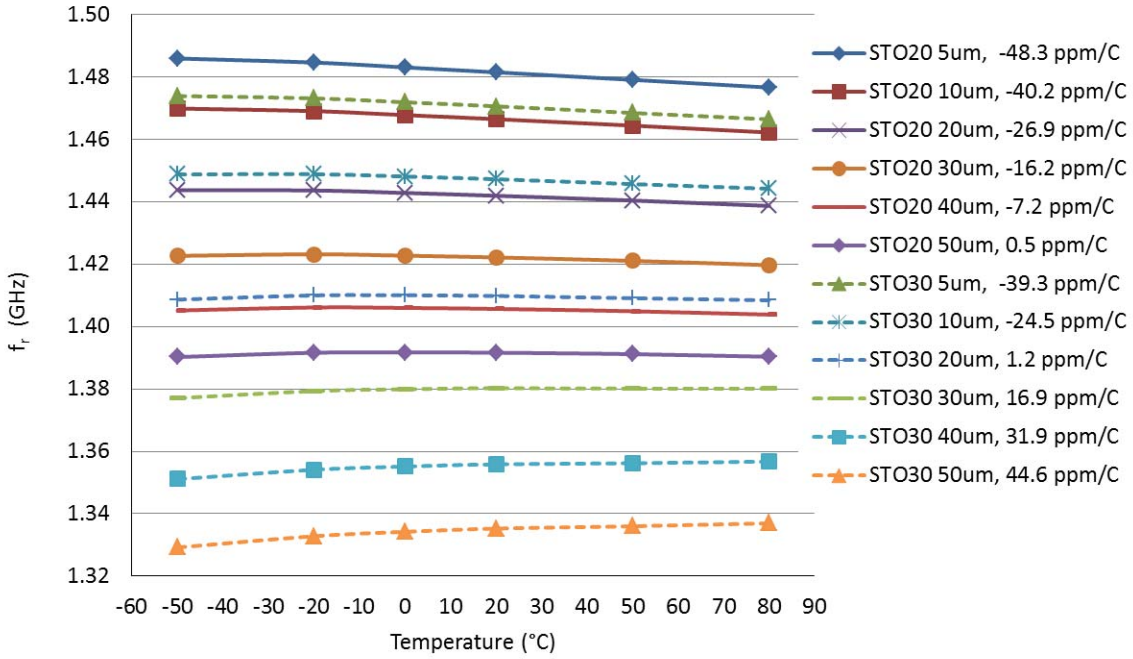

Figure 15. Simulated f_r of SL resonators as a function of temperature at STO layer thicknesses of 5 to 50 μm. τ_f data are shown in legend.

For CMB STO30, there is a crossover thickness where the τ_f changes polarity from negative to positive as thickness increases. The crossover thickness is about 20 μm where the simulated τ_f is equal to 1.2 ppm/°C. The simulation is consistent with the experiment in which a τ_f of 0.5 ppm/°C is measured at 20 μm (Table 6). Again, the simulation underestimates τ_f at thicker STO layers, as evidenced by the simulated τ_f of 31.9 ppm/°C versus the measured 60.8 ppm/°C at the same 40 μm CMB STO30 thickness. The cause of the underestimation is not clear at the moment, and warrants further investigation.

4.4.2. Effect of STO configurations

Figure 16 compares the temperature and thickness dependence of ε_{eff} for CMB STO30 between cases 1 and 2. The ε_{eff} is higher in case 1. For example, at 20 °C and 5 μm thick, the ε_{eff} is 8.20 in case 1, and 7.91 in case 2, which is an increase of ~ 3.5%. Similar increase in ε_{eff} is observed at all temperatures and CMB STO30 thicknesses for case 1. The results indicate that the SL sees more of the CMB STO30 when the material is placed next to it, compared to the configuration where the same material is placed one LTCC tape layer away.

The relative change in ε_{eff} with STO30 thickness is also more substantial in case 1. For example, at 20 °C, the ε_{eff} is 8.20 at 5 μm, and 9.94 at 50 μm, which is an increase of ~ 21.2%. In contrast, for case 2, the ε_{eff} is 7.91 at 5 μm, and 8.17 at 50 μm, which is an increase only of ~ 3.3%. Certainly, for τ_f compensation by adjusting the amount of STO30, the result is more pronounced when the compensating dielectric is integrated next to the SL resonator.

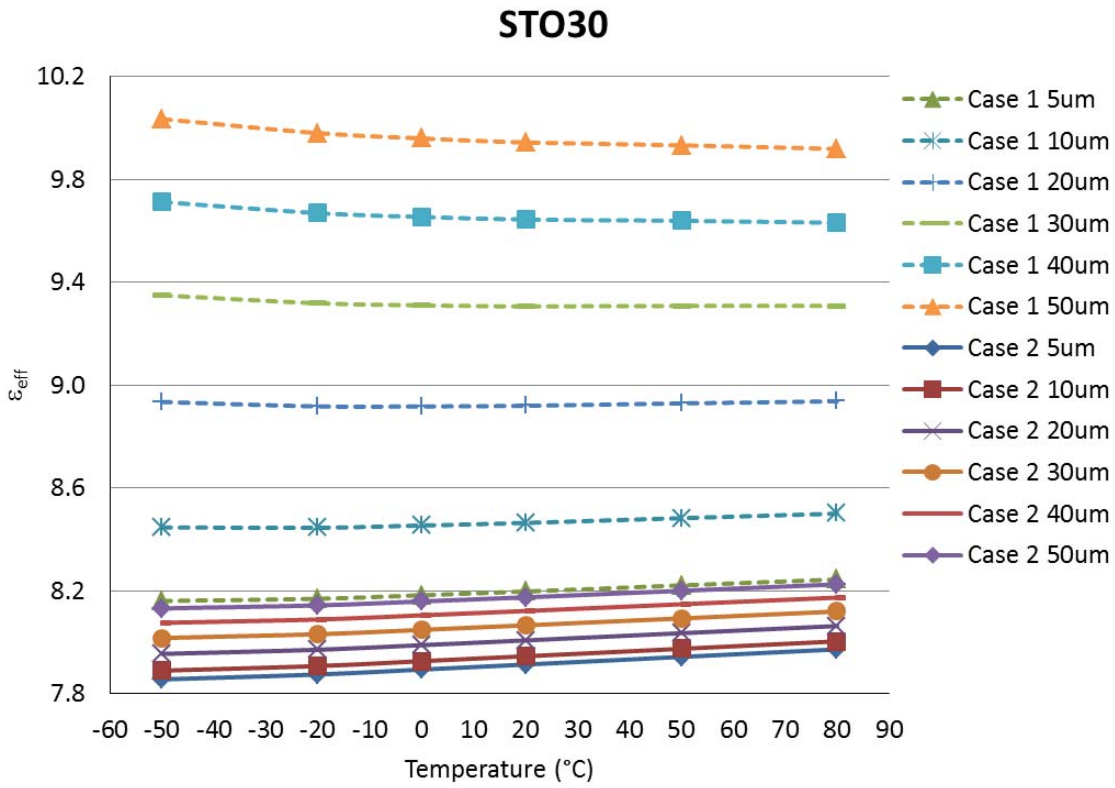

Figure 16. ε_{eff} of STO30 as a function of temperature for cases 1 and 2.

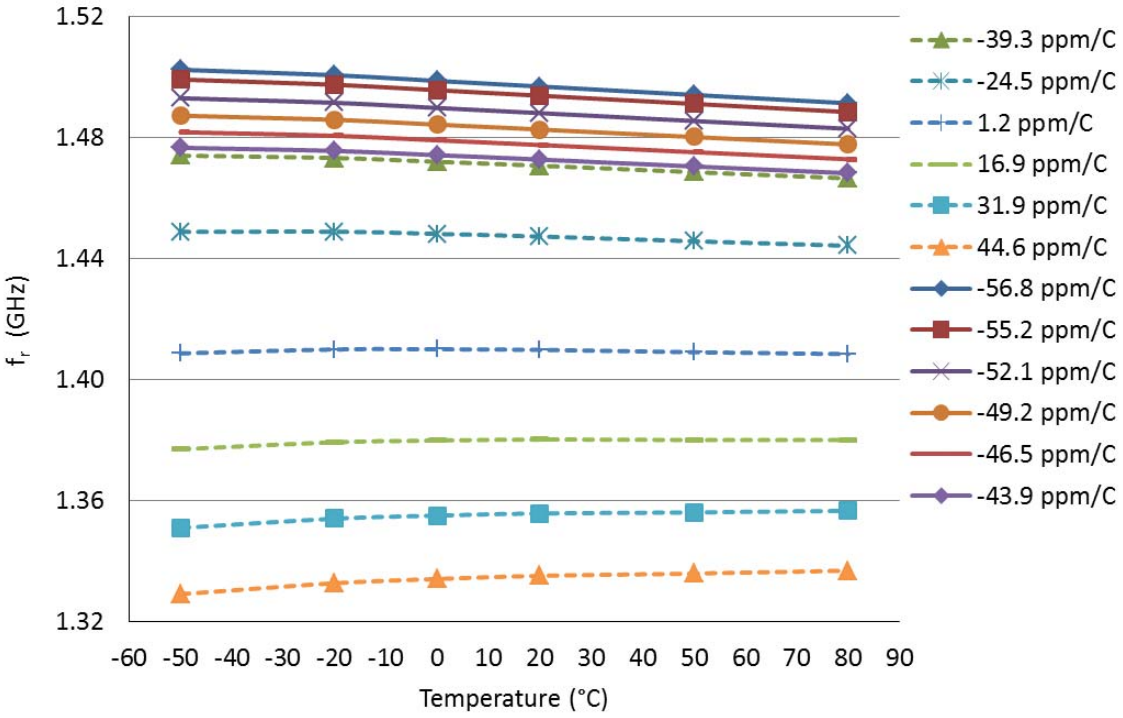

Figure 17. f_r of STO30 as a function of temperature for cases 1 and 2.

Both of these effects are reflected in the simulated f_r over temperature in Figure 17 with the corresponding τ_f shown in the legend. For the CMB STO30 in case 1, the τ_f reaches 1.2 ppm/°C at a thickness of 20 µm. For the same thickness in case 2, the τ_f is calculated as -52.1 ppm/°C. In fact, in case 2, the τ_f does not have a crossover point where it changes polarity, as evidenced by the negative slope of all $f_r \sim T$ curves at STO thicknesses from 5 to 50 µm. Rather, the τ_f remains negative, and only drops to -43.9 ppm/°C at a thickness 50 µm. In short, when placed one LTCC tape layer away from the SL resonator, the CMB STO30 does not effectively adjust the τ_f of the resonator to 0 ppm/°C.

Similar analysis is extended to CMB STO30 in case 3, where the STO layer is two LTCC tape layers away from the SL. The τ_f compensation in this configuration is even less effective than that in case 2. As expected, the analysis also shows the CMB STO20 has less effect on τ_f adjustment than CMB STO30 for both cases 2 and 3. The simulated τ_f for cases 1, 2 and 3 using CMB STO20 and CMB STO30 at thicknesses of 5 to 50 µm are plotted in Figure 18. It is clear that, only in case 1, does the τ_f reach 0 ppm/°C. For both cases 2 and 3, the effect of STO on the adjustment of τ_f is very limited, and far from reaching 0 ppm/°C, as evidenced by the clustering of τ_f data points in a -40 and -60 ppm/°C range. Figure 18 also includes the measured τ_f data for case 1. The simulated τ_f fit the experimental data well at a layer thickness of 20 µm for both STOs. However, the simulation underestimates the τ_f for the 40 µm layer.

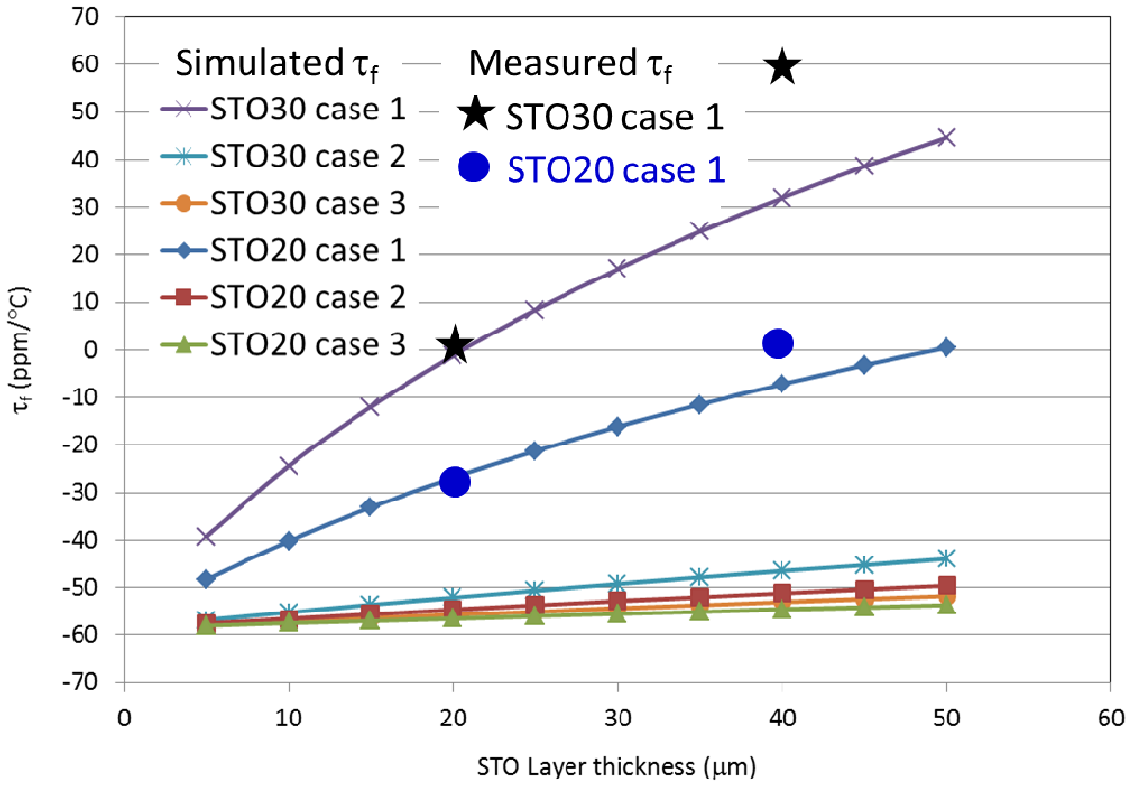

Figure 18. τ_f of SL resonators from simulation (solid lines) and experiment (discrete points).

4.5. Mechanisms of Effective τ_f Compensation

In this section we try to explain the effectiveness of τ_f compensation in case 1 by addressing energy distribution in a heterogeneous dielectric multilayer structure. The discussion is based more on physical principles rather than detailed analytical analysis.

4.5.1. Energy filling factor

The overall τ_f of a dielectric composite is given by [7]:

$$\tau_f = \sum_i P_i \tau_{fi} \quad (14)$$

where τ_{fi} is the temperature coefficient of resonant frequency of dielectric i, and P_i, the electromagnetic (EM) energy filling factor, which is the fraction of the total energy confined within the volume occupied by dielectric i. P_i is determined by the dielectric constant, volume, and geometry of dielectric i, as well as the EM field distribution inside the dielectric.

For a dielectric composite with simple geometry, such as a cylindrical puck with alternating layers of two dielectrics, the calculation of P_i is straight forward [7, 8]. However, for a SL with a finite conductor width inside a multilayer dielectric, such as the integration of dissimilar τ_f compensating dielectrics in a host LTCC dielectric, the calculation of P_i is complicated by the complex EM field distribution, as well as the reflection/refraction of EM waves at the dielectric interfaces.

4.5.2. Energy concentration in STO dielectrics in case 1

The total sintered thickness of a 4-tape 951 LTCC panel is 0.844 mm, resulting in a distance of 0.422 mm between the SL and the ground planes. At a line width of 0.2 mm, the aspect ratio of the "SL capacitor" is less than ½. Hence the electric field distribution between the SL and the ground plane is very different from an ideal parallel plate capacitor (which typically has an aspect ratio ≥ 10), in which the electric field is confined within the capacitor dielectric with no or minimum fringing effect. Rather, the fringing electric field of the SL in this study dominates the field distribution.

With the STO layers next to the SL, the oblique incidence of the fringing electric field at the STO-LTCC dielectric interface follows Snell's law. Using the CMB STO30 as an example, the dielectric constant $\varepsilon_{STO30} = 15.76$ is twice the $\varepsilon_{LTCC} = 7.88$ at 20 °C, so there is an existence of a critical, or total internal reflection, angle θ_c,

$$\theta_c = \text{asin}\left(\frac{n_{LCTT}}{n_{STO30}}\right) = \text{asin}\left(\frac{\sqrt{\varepsilon_{LTCC}}}{\sqrt{\varepsilon_{STO30}}}\right) = 45° \quad (15)$$

where n_{LTCC} and n_{STO30} are the refractive indices of the 951 LTCC and STO30, respectively. At an incident angle lower than θ_c, part of the fringing electric is reflected back to the STO30, and part is transmitted into the LTCC. At an incident angle higher than θ_c, the fringing field is totally reflected back to the STO layer. The partial and total reflections of the field at the STO-LTCC interface confine a disproportionally higher amount of electric energy within the STO layers.

According to equation (14), the higher energy filling factor, P_{STO}, amplifies the contribution from the STO, while the relatively lower P_{LTCC} reduces the effect from the 951 LTCC. This combination results in a much more effective τ_f compensation when a STO is placed next to the SL.

For cases 2 and 3, the oblique incidence of the fringing electric field at the LTCC-STO interface do not lead to a total reflection of the field inside the STO layers at any incident angle, since the EM waves hit the interface from the side having a lower dielectric constant. The energy in the STO is equal to $\frac{1}{2} \varepsilon_{STO30} E^2 * V_{STO}$, where E is the electric field transmitted through the STO layers, and V_{STO} is the volume of STO. For a STO layer thickness of 40 μm, its volume fraction is fairly small compared to the volume of the 422 μm thick LTCC. The τ_f of the SL resonator is, thus, largely dominated by the τ_f of the 951 LTCC.

5. CONCLUSIONS

We have demonstrated that, with the design of proper τ_f compensating materials and successful cofiring of the materials with DuPont 951 LTCC, SL resonators having a near zero τ_f can be produced. The compensation of the τ_f is realized locally inside a LTCC structure where the resonators reside. Among the examined titanate materials, $SrTiO_3$ is the best τ_f adjuster due to its higher τ_ε. The adjustment of τ_f scales with the amount of a titanate in a compensating material, as well as the thickness of the screen printed compensating material. More importantly, the most effective compensation of τ_f is achieved by incorporating a given compensating material next to the SL resonator. τ_f compensation is diminished when the compensating material is placed away from the SL. The electric energy concentration at the compensating layers surrounding the SL is attributed to the effectiveness of the τ_f compensation. EM simulation of τ_f using ε_{eff} calculated using a variational method confirms the experimental observation.

6. REFERENCES

1. C. Wang and K. A. Zaki, "Temperature Compensation of Combline Resonator and Filters", IEEE MMT-S Intern. Microwave Sump, Digest 3, pp 1041-1044, 1993.

2. H. Johnson and A Tunumen, "Temperature Compensated Dielectric Filter", U S Patent 5302924, 1994.

3. R. C. Kell, A. C. Greenham and G. C. E. Olds, "High-Permittivity Temperature-Stable Ceramic Dielectrics with Low Microwave Loss", J. Am. Ceram Soc, Vol 56, pp 352-354, 1973.

4. S. Kucheiko, J, Choi, H. Kim, H. Jung, "Microwave Dielectric Properties of $CaTiO_3$-$Ca(Al_{1/2}Ta_{1/2})O_3$ Ceramics", J. Am. Ceram Soc., Vol 79, pp 2739-43, 1996.

5. W. Wersing, "Microwave Ceramics for Resonators and Filters", Solids State and Mat Sci, 1(5), pp 715-731, 1996.

6. I. M. Reaney and D. Iddles, "Microwave Dielectric Ceramics for Resonators and Filters in Mobile Phone Networks", J. Am. Ceram Soc., 89, pp 2063-2072, 2006.

7. N. Alford, J. Breeze, S. Penn and M. Poole, "Layered Al_2O_3-TiO_2 Composite Dielectric Resonators With Tunable Temperature Coefficient for Microwave Applications", IEE Proc-Sci. Meas. Technol., Vol. 147, No. 6, pp 269-273, 2000.

8. L. Li and X. M. Chen, "Adhesive-Bonded $Ca(Mg_{1/3}Nb_{2/3})O_3$/$Ba(Zn_{1/3}Nb_{2/3})O_3$ Layered Dielectric Resonators with Tunable Temperature Coefficient of Resonant Frequency", J. Am. Ceram. Soc., 89, pp. 544-549, 2006.

9. S. Dai, R. Huang and D. Wilcox, "Use of Titanates to Achieve a temperature Stable Low Temperature Cofired Ceramic Dielectric for Wireless Applications", J. Am. Ceram, Soc, 85, pp 828-832, 2002.

10. H. Jantunen, "Temperature Coefficient of Microwave Resonance Frequency of a Low-Temperature Cofired Ceramic (LTCC) System", J. Am. Ceram, Soc, 85, pp 697-699, 2002.

11. H. Kapta, T. Inoue and J. Kato, "Low Fire Bismuth Based Dielectric Ceramics for Microwave Use", Jpn. J. Appl. Phy., 31, pp 3152-55, 1992.

12. Y. Choi, J. Park, J. G. Park, "Middle-permittivity LTCC Dielectric Compositions With Adjustable Temperature Coefficient", Materials Letters, 58, pp 3102-3106, 2004.

13. A. J. Moulson and J. M. Herbert, Electroceramics, Chapman & Hall, p 234, 1990.

14. E. Yamashita, "Variational method for the analysis of microstrip-like transmission lines," IEEE Trans. Microwave Theory Tech, vol. 16, no. 8, pp. 529-535, Aug. 1968.

15. R. Crampagne, M. Ahmadpanah, and J.-L. Guiraud, "A simple method for deterring the green's function for a large class of MIC lines having multilayered dielectric structures," IEEE Trans. Microwave Theory Tech, vol. 26, no. 2, pp. 82-87, Feb. 1978.

16. Y. Chang and I. C. Chang, "Simple method for the variational analysis of a generalized N-dielectric-layer transmission line," Electron. Lett., vol. 6, no. 3, pp. 49-50, Feb. 1970.

17. B. Bhat and S. K. Koul , "Stripline-like transmission lines for microwave integrated circuits", New Delhi: New Age International, p. 77. 2011.

18. A. Mohanram, G. L. Messing, and D. J. Green, "Densification and Sintering Viscosity of Low-Temperature Co-Fired Ceramics", J. Am. Ceram. Soc., 88 [10], pp 2681-2689, 2005.

19. S. Dai, "Densification and crystallization in crystallizable low temperature co-fired ceramics", Journal of materials Sciences. Published online Feb 18, 2012. Print version TBD.

DISTRIBUTION

External distribution

1 Microelectronics Engineering National Nuclear Security Administration's Kansas City Plant Operated by Honeywell Federal Manufacturing & Technologies, LLC
Attn: Dan Krueger
P.O. Box 419159
Kansas City, MO 64141-6159

Sandia distribution

1	MS0959	Adrian Casias	01832
1	MS0959	Kenneth Peterson	01832
1	MS0348	Christophe Rodenbeck	05352
1	MS0348	Richard Knudson	05353
1	MS0899	Technical Library	9536 (electronic copy)
1	MS0359	D. Chavez, LDRD Office	1911


Sandia National Laboratories